Extended Functionalities of Photovoltaic Systems with Flexible Power Point Tracking

Recent Advances

Tafti, H. Dehghani; Konstantinou, G.; Townsend, C. D.; Farivar, G. G.; Sangwongwanich, A.; Yang, Y.; Pou, J.; Blaabjerg, F.

Published in:
IEEE Transactions on Power Electronics

DOI (link to publication from Publisher):
10.1109/TPEL.2020.2970447

Publication date:
2020

Document Version
Accepted author manuscript, peer reviewed version

Extended Functionalities of Photovoltaic Systems with Flexible Power Point Tracking: Recent Advances

Hossein Dehghani Tafti, *Member, IEEE,* Georgios Konstantinou, *Senior Member, IEEE,*
Christopher D. Townsend, *Member, IEEE,* Glen G. Farivar, *Member, IEEE,*
Ariya Sangwongwanich, *Member, IEEE,* Yongheng Yang, *Senior Member, IEEE,*
Josep Pou, *Fellow, IEEE,* and Frede Blaabjerg, *Fellow, IEEE*

***Abstract*—The power system is experiencing an ever-increasing integration of photovoltaic power plants (PVPPs), which leads demand on the power system operators to force new requirements to sustain with quality and reliability of the grid. Subsequently, a significant quantity of flexible power point tracking (FPPT) algorithms have been proposed in the literature to enhance functionalities PVPPs. The intention of FPPT algorithms is to regulate the PV power to a specific value imposed by the grid codes and operational conditions. This will inevitably interfere the maximum power point tracking (MPPT) operation of PV systems. Nevertheless, the FPPT control makes PVPPs much more grid-friendly. The main contribution of this paper is to comprehensively compare available FPPT algorithms in the literature from different aspects and provide a benchmark for researchers and engineers to select suitable FPPT algorithms for specific applications. A classification and short description of them are provided. The dynamic performances of the investigated algorithms are compared with experimental tests on a scaled-down prototype. Directions for future studies in this area are also presented.**

***Index Terms*—Active power control, constant power generation, flexible power point tracking, photovoltaic systems, power curtailment control, power reserve control.**

I. Introduction

Renewable energy resources have experienced a drastic increase in the electricity generation market because of fast developing economies and industries. Among various types of renewable energy resources, wind and solar energy achieved higher growth thanks to their reduced environmental impact and abundance. Due to the reduction of photovoltaic (PV) panels cost, the growth rate of installation of PV power plants (PVPPs) is greater than that of wind power systems [1], [2]. The installed PV capacity was increased by 98 GW in 2017, while it was incremented with additional capacity of 109 GW in 2018 (more than twice the capacity installed in 2015) [3].

The most important concern for both utility and residential scale PVPP owners is to maximize their revenue, in which cost and efficiency are critical parameters. It is seen from the power-voltage (P-V) curve of a PV string in Fig. 1 that there is a unique operating point where the PV array power is maximized. The P-V characteristics of PV strings are affected by variations of solar irradiance, temperature, and aging. Therefore, an algorithm to extract the maximum power from the PV string is required. Maximum power point tracking (MPPT) algorithms are normally employed to set the operation point of the PV string at the maximum power point (MPP, in Fig. 1) by regulating the PV voltage at v_{mpp} [4], [5]. There are several MPPT algorithms available in the literature with their own advantages and disadvantages. Comprehensive comparisons and reviews on various MPPT algorithms for PVPPs have been discussed in [6]–[9]. The most frequently-applied MPPT algorithms are the perturb and observe (P&O) [10]–[12] and incremental conductance (INC) algorithms [13], [14]. Key features of MPPT algorithms include: accuracy of tracking the MPP, computational complexity, dynamic performance, and steady-state power oscillations.

Countries with a significant amount of installed renewable energy sources may face several challenges in the near future. For instance, if the amount of the generated power from renewable energy sources exceeds the load demand during peak power generation periods, the power system may be overloaded and subsequently protection devices may be triggered [2], [15], [16]. In order to ensure the stability and quality of the power system, power system operators continually update the requirements for PVPPs for the connection to the grid [17]–[22], referring to as grid codes and standards, which aim to reduce the adverse effects of the high penetration of installed PVPPs in the power system.

A common theme of all new and updated grid codes is grid-support functionality with flexibility to inject an amount of

Manuscript received August 12, 2019; revised December 17, 2019; accepted January 21, 2020. This work was supported by the Singapore Ministry of Education Academic Research Fund Tier 1 under Grant No: 2019-T1-001-168 (RG80/19).

H. D. Tafti and J. Pou are with the School of Electrical and Electronic Engineering, Nanyang Technological University, 639798 Singapore (e-mail: hossein002@e.ntu.edu.sg; josep.pou@ieee.org).

G. Konstantinou is with the School of Electrical Engineering and Telecommunications, University of New South Wales, Sydney, NSW 2052, Australia (e-mail: g.konstantinou@unsw.edu.au).

C. D. Townsend is with the Department of Electrical, Electronic, and Computer Engineering, The University of Western Australia, Crawley WA 6009, Australia (e-mail: townsend@ieee.org)

G. G. Farivar is with the Energy Research Institute, Nanyang Technological University, 639798 Singapore (e-mail: gh_farivar@hotmail.com).

A. Sangwongwanich, Y. Yang and F. Blaabjerg are with the Department of Energy Technology, Aalborg University, Aalborg 9220, Denmark (e-mail: ars@et.aau.dk; yoy@et.aau.dk; fbl@et.aau.dk)

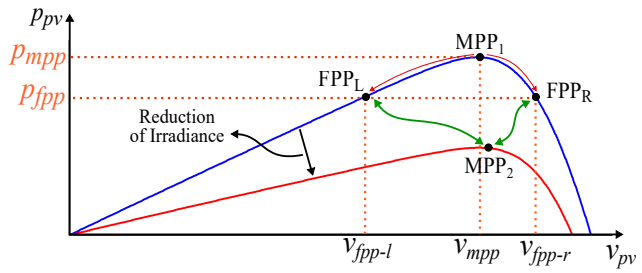

Fig. 1. Maximum and flexible power point tracking in PVPPs (MPP - Maximum power point; FPP - Flexible power point).

active and reactive power based on grid conditions [23]. Power limiting control (constant power generation - CPG) [24]–[26], power reserve control [27]–[29], absolute active power control [18], [30], [31], reduced power control [32], [33], delta power control [34] and power ramp-rate control [35], [36] requirements are some examples of these new regulations. In order to fulfill these requirements, the concept of flexible power point tracking (FPPT) is becoming mandatory in PVPPs, in addition to the conventional MPPT algorithms [37]. In this paper, the FPPT is used as a general term to describe all forms of active power control, which have been presented in the literature with various names.

During the FPPT operation mode (see Fig. 1), the extracted power from the PV strings is adjusted according to the power reference p_{fpp}. If the power reference p_{fpp} is smaller than the maximum available power, the operation point of the PV string can be moved to the right- or left-side of the MPP ($\mathrm{FPP_R}$ or $\mathrm{FPP_L}$). Moreover, if the available power from the PV string is smaller than the power reference, it extracts the maximum available power by operating the system at $\mathrm{MPP_2}$.

Several FPPT algorithms have been proposed in the literature. Some of these algorithms require extra energy storage, capacitor, etc., to provide flexible power control in PVPPs [38]–[44]. However, the selected algorithms in this paper can provide these features for PVPPs by changing the operation point of the PV strings, instead of adding extra components into the system. This paper provides a broad view and a comprehensive comparison of the available FPPT algorithms for PVPPs. The main contribution of this paper is to classify the state-of-the-art FPPT algorithms and compare their performance, advantages and disadvantages in various aspects. The performance of these algorithms is also experimentally tested and the results are compared under various operational conditions.

The remainder of this paper is structured as follows. The motivations of the FPPT operation, including various grid codes and standards, which necessitate the FPPT operation for PVPPs are summarized in Section II. The overall control algorithms for various types of PVPPs are described in Section III. The details of several FPPT algorithms from the literature are given in Section IV and their performances are compared experimentally in Section V. Finally, a comprehensive comparison between the selected FPPT algorithms is provided in Section VI, and the concluding remarks and future research perspectives are given in Section VII.

TABLE I
VARIOUS GRID CODES AND STANDARDS FOR PVPPS

Country	Title
Australia	Grid-connected PV systems: Design and installation training manual [45]
Denmark	Technical regulation 3.2.2 for PV power with power output above 11 kW [19]
Germany	Generating plants connected to the medium-voltage network [46]
South Africa	Grid connection code for renewable power plants connected to the electricity transmission system or the distribution system in South Africa [47]

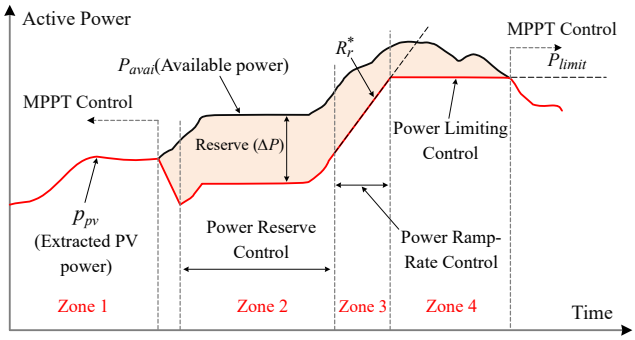

Fig. 2. Various operation modes of PVPPs with active power control [19].

II. MOTIVATIONS FOR THE FPPT OPERATION IN PVPPS

Various countries have different regulations and standards for the operation of PVPPs. In this section, standards and grid codes of four countries (i.e., Australia, Denmark, Germany, and South Africa) are described, as mentioned in Table I.

Active power control is divided into several requirements, as shown in Fig. 2. These are explained in the following.

- *Zone* 1 - *MPPT control*. MPPT operation is implemented in this zone, which extracts the maximum power from the PV strings. During this operation mode, the active power of the inverter is not regulated by the grid codes, but it depends on the maximum available power from the PV strings.
- *Zone* 2 - *Power reserve constraint (delta power constraint).* A delta power constraint is used to limit the active power from a PVPP to a desired constant value in a proportion of the maximum available power. A margin is kept as a reserve (ΔP) between the available maximum power of the PVPP and the injected power to the grid. A delta power constraint is typically used to establish a regulating reserve for an upward increase of the power in connection with the frequency support. The regulations by various international grid codes are depicted in Fig. 3. When the grid frequency is within the frequency control band (f_2 and f_3), a power reserve value of ΔP is considered between the extracted

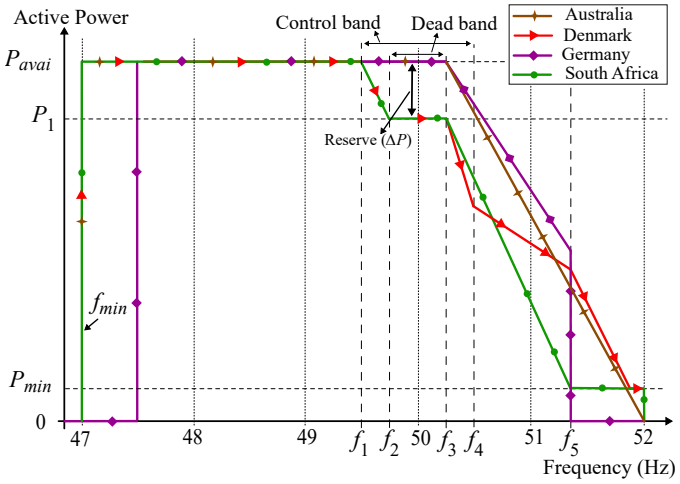

Fig. 3. Frequency support regulations by international grid codes [19], [45]–[47].

PV power and its maximum available power (Zone 2 in Fig. 2). This enables the PVPP to increase the output power to the maximum available power (P_{avai}) if the grid frequency drops below f_2. If the frequency is between 47 Hz and f_1, the PV system should inject the maximum power P_{avai} to the grid. On the other hand, for frequencies larger than the upper limit of the frequency band f_3, the PV power reduces based on droop relationship, defined in the standard. When the grid frequency is larger than 52 Hz, the PV system should cease the power generation and be disconnected from the grid.

- *Zone* 3 - *Ramp rate constraint.* A ramp rate constraint is used to limit the power ramp rate by which the active power can be changed. According to frequency-power characteristics, under fast environmental changes, the rate of the PV power change should be limited to a specific value R_r^*, defined by the grid codes. This requirement helps to retain the stability of the power system.
- *Zone* 4 - *Power limiting control (absolute power constraint).* An absolute power constraint is typically used to protect the power system against overload in critical situations. As depicted in Fig. 3, if the available PV power is larger than the inverter maximum power (P_{limit}), the PV power is kept as constant. In addition, the injected power to the grid remains constant for a longer period of time, which can improve the quality and reliability of the power system.

Based on the above-mentioned grid requirements, flexible power control is necessary in PVPPs in order to achieve active power control and frequency support. The grid requirements are not limited to active power control. They also govern reactive power control and voltage support, which is discussed in the following subsection.

III. System Topologies

PVPP systems are divided into two categories, as depicted in Fig. 4. In the single-stage configuration, a grid-connected inverter is directly connected to the PV strings and all of the

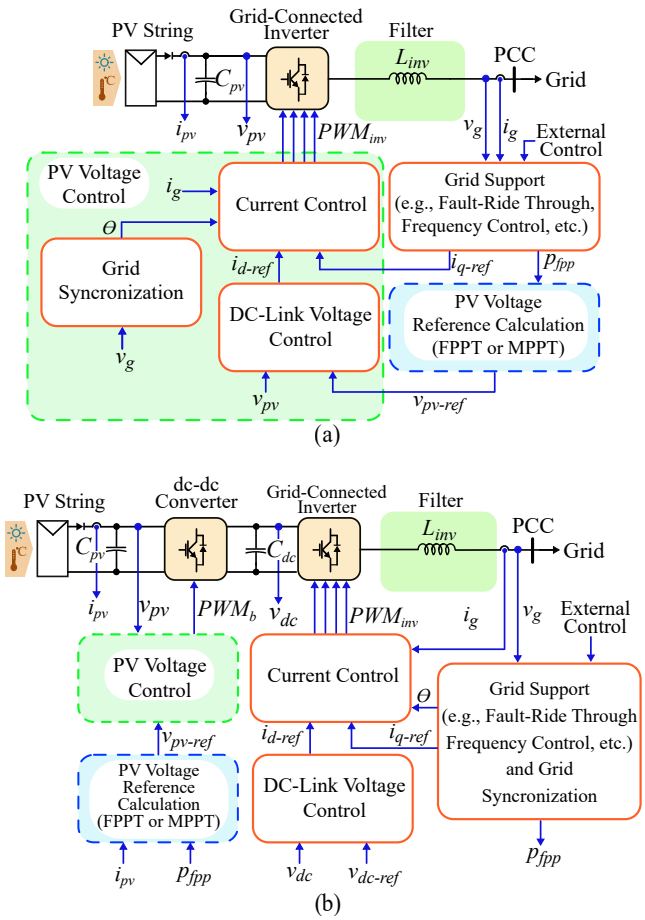

Fig. 4. Photovoltaic power plant structures: (a) Single-stage, and (b) two-stage system.

control functionalities are implemented on this inverter [48], as shown in Fig. 4(a), where the control blocks have the following functionalities:

- Grid Support provides fault ride-through (FRT) capability, frequency support, power ramp-up/down control, etc. for the PVPP. It calculates the active/reactive power reference (p_{fpp} and q_{ref}) for the inverter, according to the operational condition and grid requirements.
- Grid Synchronization typically includes a phase-locked-loop (PLL) to calculate the grid voltage angle and synchronize the inverter current with the grid.
- PV Voltage Reference Calculation (FPPT or MPPT) calculates the PV voltage ($v_{dc\text{-}ref}$), related to the power reference, as illustrated in Fig. 1(b). It is the main focus of this paper and different available algorithms will be presented.
- DC-link Voltage Control. In the single-stage PVPP, the PV strings are directly connected to the dc-link, and thus the dc-link voltage is equal to the PV string voltage. Consequently, the voltage reference, calculated by the FPPT block, is used as the input of the dc-link voltage controller. The output of this block is the current reference ($I_{dq\text{-}ref}$), which is fed to the current controller.
- Current Control. Various current control strategies, like proportional-integral (PI) controller [49] and proportional resonant (PR) controller [50] can be implemented in this

block in order to regulate the inverter current to its reference.

In the two-stage configuration, a dc-dc converter is connected between the PV strings and the dc-link, as shown in Fig. 4(b). The dc-dc converter controls the PV voltage according to the voltage reference $v_{pv\text{-}ref}$, which is calculated by the FPPT or MPPT block. The grid support requirements are implemented in the inverter controller, in which the PV power reference p_{fpp} is also calculated.

IV. Flexible Power Point Tracking Algorithms

A short description of the available FPPT algorithms in the literature is provided in this section. These algorithms can be divided into two types:

Type A) The controller of the connected converter to the PV string (dc-dc converter in two-stage PVPPs and dc-ac inverter in single-stage PVPPs) is modified in order to regulate the PV power to its reference value [49], [53], [54], [60]–[65]. In these algorithms, the "PV Voltage Control" block, shown in Fig. 4(b), is modified, while a conventional MPPT algorithm is implemented in the "PV Voltage Reference Calculation" block. In order to achieve the FPPT operation, the calculated voltage reference by the MPPT algorithm is modified in the "PV Voltage Control" block.

Type B) Algorithms with the direct calculation of the PV voltage reference corresponding to the power reference p_{fpp}. In these algorithms, the "PV Voltage Control" block, shown in Fig. 4(b), remains as any conventional voltage control algorithm, while an FPPT algorithm is implemented as the "PV Voltage Reference Calculation" block [24], [25], [28], [32], [58], [59]. The FPPT algorithm calculates $v_{pv\text{-}ref}$ based on the PV power reference p_{fpp}. The PV voltage controller regulates the PV voltage to its reference $v_{pv\text{-}ref}$, which consequently regulates the PV power to its reference p_{fpp}.

The details of these FPPT algorithms are provided in the following subsections.

A. Type A: Algorithms with Modification of the PV Voltage Controller

The available algorithms in the literature in *Type A* can further be categorized into eight methods (Fig. 5) and detailed in the following.

Method 1 *(m*1*):* This FPPT algorithm directly controls the active power [51], [52] (Fig. 5(a)). The instantaneous PV power is compared with its reference and the error is fed into a PI controller, which calculates the switching duty cycle of the dc-dc converter. However, this algorithm is not able to extract the maximum power from the PV strings. The PV operation point moves to the right-side of the MPP, which results in larger power oscillations. This algorithm does not contain the "PV Voltage Reference Calculation" block and is not able to track the MPP if the power reference p_{fpp} is larger than the available maximum power (see Fig. 1).

Method 2 *(m*2*):* A multi-mode FPPT algorithm with the calculation of the PV current reference i^*_{pv} based on the ratio of the power reference p_{fpp} and instantaneous PV power p_{pv} was proposed in [53] (Fig. 5(b)). The ratio $\frac{p_{fpp}}{p_{pv}}$ is multiplied by the instantaneous PV current i_{pv} resulting in the PV current reference i^*_{pv}. With $p_{fpp} > p_{pv}$, i^*_{pv} increases, which increases the PV power in the left-side of the MPP; and vice versa. At steady state, $p_{fpp} \simeq p_{pv}$, and accordingly, i^*_{pv} remains close to i_{pv}. A dc-link voltage stabilizer is also implemented in the dc-dc converter in this algorithm. If the dc-link voltage is larger than its upper range, the current reference is reduced by ΔI; otherwise it increases. Finally, the modified PV current reference $i^*_{pv\text{-}1}$ is compared with its measured value i_{pv} and is fed to a PI controller to generate the duty cycle D of the dc-dc converter. The "PV Voltage Reference Calculation" block is not considered in this algorithm, and as a result, it is not able to track the MPP while the power reference is larger than the available power (see Fig. 1). Hence, this algorithm is applicable for short-term operation of the PVPPs with limited output power, but it can not properly control the PV power for long periods (e.g., including normal MPPT operation).

Method 3 *(m*3*):* An FPPT algorithm with the calculation of the current reference of the dc-dc boost converter based on the power reference p_{fpp} was introduced in [54] (Fig. 5(c)). The inductor current reference is calculated using two loops, i.e., the MPPT algorithm and power limitation algorithm. The smaller value is always chosen as the inductor current reference i^*_l. Under the power limitation operation, the MPPT algorithm is frozen and the last calculated value of the MPP voltage is used for the calculation of the inductor current reference. The inductor current reference is limited to I_{max}, which is the summation of $i^*_{l\text{-}fpp}$ and a constant current I_0 that is set based on the PV capacitor size and the inductor size. Furthermore, the calculated inductor current reference is limited to I_{max} to enable fast dynamics and avoid voltage drops after switching to the MPPT operation. This algorithm moves the operation mode to the right-side of the MPP.

Method 4 *(m*4*):* With a multi-mode operation, based on a comparison between the PV power and its reference, the FPPT controllability was obtained in [55]–[57] (Fig. 5(d)). When the PV power is smaller than the reference ($p_{pv} < p_{ref}$), the MPPT algorithm calculates the PV voltage reference v^*_{pv}, which increases the PV power. Subsequently, the duty cycle is computed using a proportional controller k_{mpp}. If the PV power is larger than the reference ($p_{pv} \geq p_{ref}$), the power limit control loop is activated and the duty cycle of the dc-dc converter is calculated based on the error between p_{pv} and p_{ref}. This operation reduces the PV power by moving the operating point to the left-side of the MPP. This operation region results in slower dynamics. Furthermore, transitions between the operation modes are necessary, which increases design complexity of the control parameters.

Methods 5 and 6 *(m*5 and *m*6*):* The FPPT algorithms in [58] are achieved by limiting the PV power or current references according to the FPPT power reference p_{fpp}, as demonstrated in Figs. 5(e) and (f), respectively. The MPPT algorithm

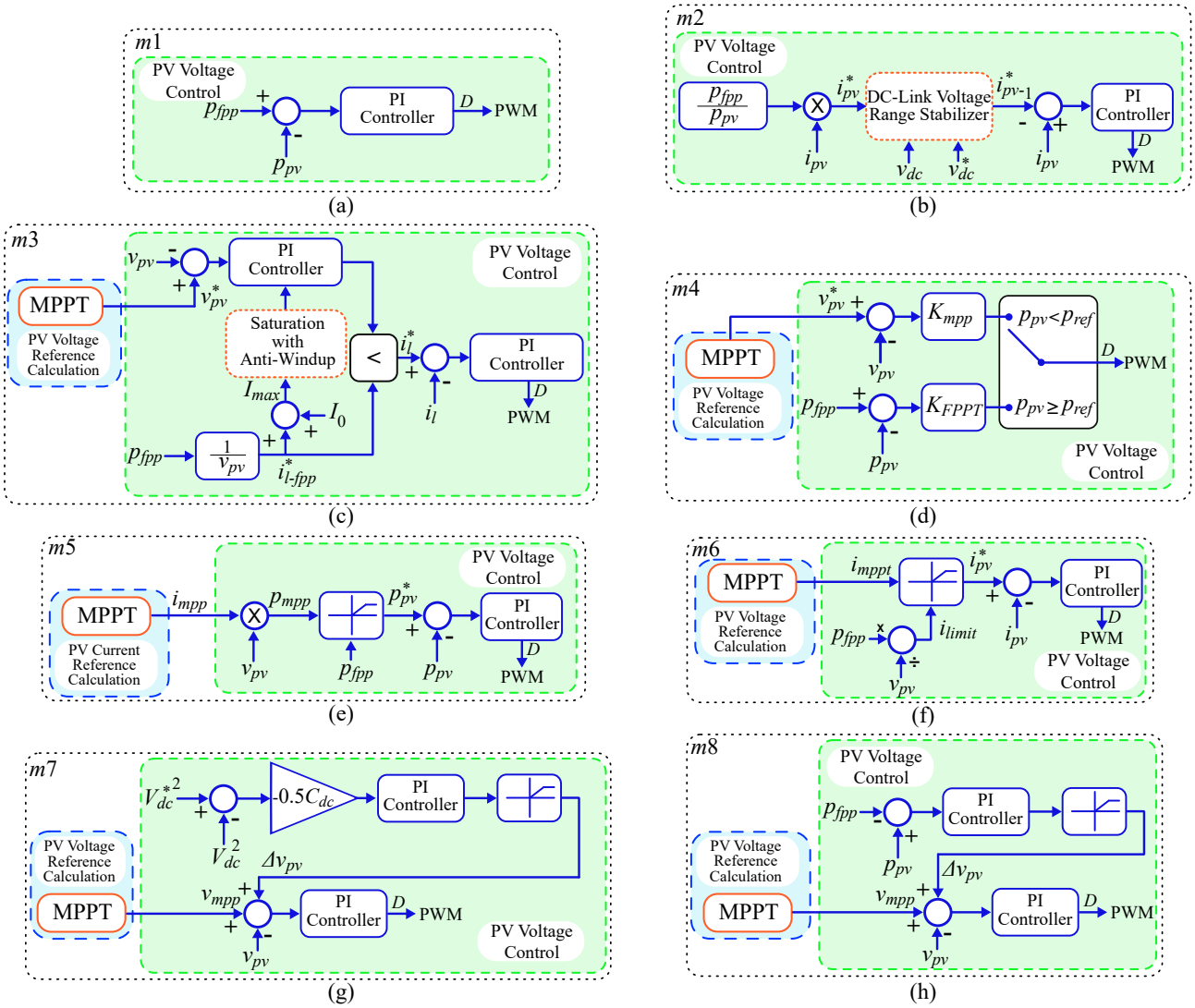

Fig. 5. *Type A* - FPPT algorithms with modification of the converter controller: (a) Method 1 (*m*1) - Direct power control [51], [52], (b) Method 2 (*m*2) - PV current control with dc-link voltage stabilizer [53], (c) Method 3 (*m*3) - PV power control with inductor current reference calculation [54], (d) Method 4 (*m*4) - multi-mode operation with PV voltage control [55]–[57], (e) Method 5 (*m*5) - PV power limit control [58], [59], (f) Method 6 (*m*6) - PV current limit control [58], [59], (g) Method 7 (*m*7) - PV power control with dc-link voltage-based delta-voltage control [49], [60], [61]; and (h) Method 8 (*m*8) - PV power control with PV power-based delta-voltage control [62].

calculates the maximum power or current under all operation modes. Subsequently, the input power or current references to the controller is limited to p_{fpp} or i_{limit}, respectively. As depicted in Figs. 5(e) and (f), i_{limit} is calculated by dividing p_{fpp} to v_{pv}. The advantage of this algorithm is that it does not require any state transitions between various operation modes. However, due to the reduction of the PV power under the power limit operation, the MPPT can produce instability and move into the wrong direction. These algorithms are able to regulate the power under environmental changes, due to the existence of the "PV Voltage Reference Calculation block", that continuously calculates the PV voltage reference with an MPPT algorithm.

Methods 7 and 8 *(m*7 and *m*8*):* In the algorithms in [49], [60]–[62], an extra amount of Δv_{pv} was added to the calculated voltage reference from the MPPT algorithm, during the power limit operation mode (Figs. 5(g) and (h)). During the MPPT operation mode, the MPPT algorithm calculates the PV voltage reference, which is fed into the controller without adding Δv_{pv}. At the beginning of the power limit operation mode, the MPPT algorithm disables and the last calculated v_{mpp} is recorded. In [49], [60], [61], the dc-dc converter of the two-stage PVPP controls the dc-link voltage during the power limit operation mode. Accordingly, Δv_{pv} is computed based on the error between the dc-link energy v_{dc}^2 and its reference value $(v_{dc}^*)^2$. The algorithm in [62] considers the power reference p_{fpp} in the calculation of Δv_{pv}. In this algorithm, the dc-link voltage is controlled using the grid-connected inverter during the power limit operation.

All of the presented algorithms in this section require modifications of the PV voltage controller, which necessitates a controller design suitable for transition changes. A compre-

hensive comparison of these algorithms is provided in Section VI.

B. Type B: Algorithms with Direct Calculation of the Voltage Reference

Algorithms with direct calculation of the voltage reference v_{fpp}, corresponding to the power reference p_{fpp}, during the FPPT operation, are investigated in this section. In these algorithms, the "PV Voltage Control" block, shown in Fig. 4, remains unchanged similar to any conventional voltage controller, while the power regulation is implemented in the "PV Voltage Reference Calculation" block. The Type B algorithms can be further categorized into three methods, as demonstrated in Fig. 6.

Method 9 *(m*9*):* The algorithms in [32], [34], [56], [66]–[68] divide the operation modes into the MPPT and FPPT operation modes (Fig. 6(a)). During the MPPT control, a conventional MPPT algorithm, e.g., P&O or INC, is implemented to calculate the PV voltage reference v_{mpp}, corresponding to the maximum available power. During the FPPT operation, a power control algorithm is implemented to calculate the voltage reference v_{fpp} corresponding to the PV power reference p_{fpp}. In order to achieve an optimum control in both modes, the voltage- and time-step values of the voltage reference calculation algorithm are set as different values. During the MPPT operation, T_{step} is set as $T_{step\text{-}mpp}$, which is relatively large (0.1 s to 1 s), while V_{step} is set as $\mathrm{V}_{step\text{-}mpp}$ that is relatively small. This set of parameters leads to small power oscillations during MPPT operation. On the other hand, $T_{step\text{-}fpp}$ is relatively small and $V_{step\text{-}fpp}$ is relatively large, in order to obtain fast transients during the FPPT operation.

Method 10 *(m*10*):* An algorithm for the calculation of the voltage-step, based on the operational condition of the PVPP (i.e. transient or steady-state), was introduced in [24] (Fig. 6(b)). During the FPPT operation, if the grid is under the *Fault* condition, a small time-step $T_{step\text{-}fpp\text{-}tr}$ and large voltage-step $V_{step\text{-}fpp\text{-}tr}$ are chosen in order to enhance the transient response. Under the *Normal* operation, the difference between the amplitude of the power reference p_{fpp} and p_{pv}, calculated as $\mid dp^* \mid = \mid p_{fpp} - p_{pv} \mid$, is compared with its threshold value dp_{th}. In this way, the operation mode is divided into steady-state or transient modes. Furthermore, a hysteresis controller is implemented to use a large voltage-step $V_{step\text{-}fpp\text{-}tr}$ and small time-step $T_{step\text{-}fpp\text{-}tr}$ under transients. The main advantages of this algorithm, compared to *m*9, include fast transients and lower power oscillations during the FPPT operation. It can be seen in Fig. 6 that even though these algorithms apply different voltage reference calculation algorithms under FPPT and MPPT operation modes, they use a similar algorithm for the calculation of the PV voltage reference v_{fpp}.

Method 11 *(m*11*):* A general algorithm for flexible power tracking in PVPPs was introduced in [69] (Fig. 6(c)). One general voltage reference calculation algorithm is implemented, which is able to calculate the voltage reference in both MPPT and FPPT operation modes. The main advantage of this algorithm, compared to the algorithms *m*9 and *m*10, is the use of a fixed time-step for all operation modes. This feature reduces the implementation complexity, as well as facilitates the tuning process for controller parameters. The use of a general algorithm for all operation modes eliminates the need for the transition changes between various operation modes of the controller. The voltage-step is calculated adaptively based on the operation mode of the PVPP, being transient or steady-state, which is identified according to the control algorithm shown in Fig. 6(c). During the steady-state operation, the aim is to reduce the power oscillations around the power reference. Therefore, the adaptive voltage step is calculated based on the derivation of the power to the voltage for that specific operation point. During the transient conditions, the objective is to achieve fast transient response. In this case, the adaptive voltage step is calculated as a proportion of the difference between the PV power and its reference. If the current operation point of the PV string is far from the reference, the voltage step is proportionally large. Once the operation point gets close to the reference, the adaptive voltage step becomes smaller, which ensures the stable operation of the PV string around the reference. More details of this algorithm can be found in [69].

V. Experimental Evaluation

A scaled-down 1.1 kVA two-stage PVPP, as shown in Fig. 4(b), has been implemented experimentally to compare the dynamic and steady-state performance of the investigated FPPT algorithms. The system consists of a three-phase grid connected inverter and a dc-dc boost converterm, as shown in Fig. 4(b). The PV panel is simulated by using a Chroma 62000H-S solar array simulator, and the grid is emulated with a Cinergia grid emulator. IMPERIX H-bridge modules are used to build the two-stage PVPP and the controller is implemented using the B-BOX RCP control platform from IMPERIX. The parameters of the experimental setup are provided in Table II.

In order to obtain a fair comparison between the algorithms, the parameters of each algorithm should be designed optimally. Due to the non-linear nature of the algorithms, an analytical solution to find the optimum values of parameters does not exist. Therefore, the sensitivity analysis tool of Matlab/Simulink is applied to find the optimum parameters numerically. A similar circuit topology with same parameters of the experimental setup is simulated. Based, on the results of the sensitivity analysis, the response optimization tool is applied to tune the parameters of algorithms optimally. In order to evaluate the algorithms the following case study is implemented. The irradiance is kept as $1000\,\mathrm{W/m^2}$ and the power reference is $p_{fpp} = 500$ W before $t = 0.15$ s. All the algorithms reach their steady-state condition at $t = 0.1$ s. Accordingly, the steady-state tracking error TE_{ss} is calculated in the following manner:

$$TE_{ss} = \frac{\int \mid p_{pv} - p_{fpp} \mid}{\int \mid p_{pv} \mid} \times 100. \tag{1}$$

In order to calculate the steady-state tracking error, the integrals in the above equation are calculated between $t =$

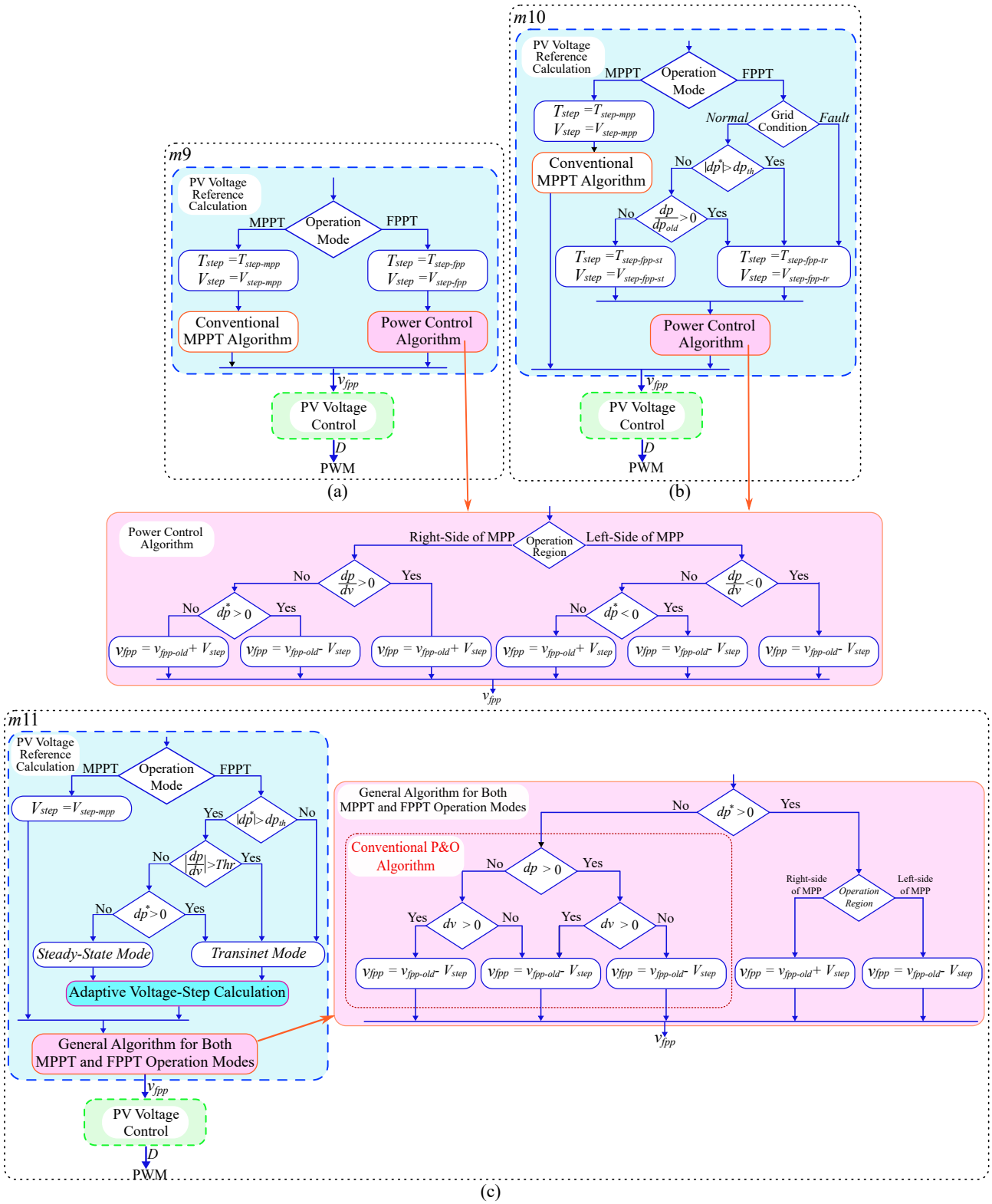

Fig. 6. *Type B* - FPPT algorithms with direct calculation of voltage reference: (a) Method 9 (*m*9) - proposed algorithms in [32], [34], [56], [66]–[68] with constant voltage-step values for MPPT and CPG, (b) Method 10 (*m*10) - proposed algorithm in [24] with different voltage-step values during transient and steady-state for MPPT, and (c) Method 11 (*m*11) - general FPPT algorithm for both MPPT and FPPT operation modes [69].

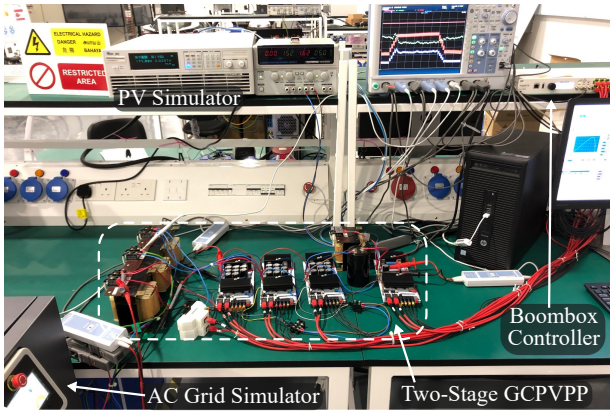

Fig. 7. Experimental setup.

$0.1\,\mathrm{s}$ and $t = 0.15\,\mathrm{s}$, in which all the algorithms operate at steady-state. In order to evaluate the transient performance of the algorithms, a step-change of the power reference from $p_{fpp} = 500$ W to $p_{fpp} = 1000$ W is implemented at $t = 0.15\,\mathrm{s}$. The transient tracking error TE_{tr} is calculated between $t = 0.15\,\mathrm{s}$ and $t = 0.22\,\mathrm{s}$, because all the algorithms reach their new steady-state condition at $t = 0.22\,\mathrm{s}$.

The optimum operation of an algorithm is when both the transient and steady-state error values are minimized. In this case, a cumulative tracking error TE is defined, as follows

$$TE = \sqrt{TE_{ss}^2 + TE_{tr}^2}. \tag{2}$$

This parameter is used as the optimization parameter for the calculation of the parameters of the algorithms.

Based on the sensitivity analysis, various trends between the parameters and tracking error values can be determined in the algorithms. For example, in m_1, the larger values of k_P (the proportional gain of the PI controller, shown in Fig. 4) result in smaller tracking error values. The same phenomena can be also seen for k_I. As another example, the larger values of integral gain k_I result in smaller values of tracking error for *m*3. Furthermore, larger values of voltage step V_{step} result in larger tracking error for *m*9-R, while by smaller values of time-step T_{step}, the tracking error can be reduced for *m*10-R. Based on this optimization strategy, the optimum values of the parameters of the algorithms are calculated and listed in Table III.

The performance of investigated algorithms is verified and compared under a fast change of the irradiance and results are demonstrated in Figs. 8 and 9. The irradiance increases from $300\,\mathrm{W/m^2}$ to $1000\,\mathrm{W/m^2}$ in the period between $t = 5\,\mathrm{s}$ and $t = 10\,\mathrm{s}$, and decreases from $1000\,\mathrm{W/m^2}$ to $300\,\mathrm{W/m^2}$ in the period between $t = 35\,\mathrm{s}$ and $t = 40\,\mathrm{s}$. Three different power reference values are considered in the evaluation of each algorithm, i.e, 75% (case I), 50% (case II) and 25% (case III) of the maximum available power of the PV string.

It should also be mentioned that to obtain a fair comparison between various FPPT algorithms, the rest of the controllers in the two-stage PVPP are considered identical. The PV simulator ensures providing similar PV curves in all the cases.

TABLE II
PARAMETERS OF THE EXPERIMENTAL AND SIMULATION SYSTEMS

Parameter	Symbol	Values
DC-link voltage	V_{dc}	250 V
Grid voltage (line-to-line)	V_g	110 V
PV maximum power*	P_{mpp}	1100 W
PV maximum power voltage	V_{mpp}	150 V
PV capacitor	C_{pv}	0.51 mF
dc-dc boost converter inductor	L_{boost}	2 mH
dc-dc switching frequency	$f_{sw\text{-}boost}$	10 kHz
Grid-connected inverter filter	L_{inv}	5 mH
Inverter switching frequency	$f_{sw\text{-}inv}$	10 kHz

* Irradiance = $1000\,\mathrm{W/m^2}$ and Temperature = $25\,^\circ\mathrm{C}$.

The algorithms *m*1 and *m*2 do not contain the "PV Voltage Reference Calculation" block (see Fig. 4) and cannot regulate the PV power under environmental changes, and hence none of them are evaluated in this experimental study. The algorithms *m*3 and *m*4 are based on a multi-mode operation and result in similar performance under environmental changes, and therefore, only *m*4 is tested. Between the algorithms *m*5 and *m*6 with limitation of the power/current reference, the method *m*6 is implemented. The algorithms *m*7 and *m*8 are not able to regulate the PV power under environmental changes, because they assume that the MPP voltage remains constant during the FPPT operation, which is not true under environmental changes. As a result, these algorithms (*m*7 and *m*8) are not analyzed in this case study. The algorithms *m*9, *m*10 and *m*11 are able to move the operating point to both the left- and right-side of the MPP and consequently the performances on both sides are evaluated. It should be remarked that the performance of *m*10 is similar to *m*9, and accordingly, *m*9 is only evaluated. It should be noted that the parameters of the inverter (like grid current and grid voltage) are not the main focus of this paper and they are not included in the results.

The performance of the algorithm *m*4 under the above-mentioned test condition is evaluated and results are illustrated in Fig. 8(a). Before $t = 5\,\mathrm{s}$, the available power is extracted from the PV string in the Cases I and II, while the PV power is regulated at 25% of the maximum power in Case III. During the interval between $t = 5\,\mathrm{s}$ and $t = 10\,\mathrm{s}$, the irradiance increases and, accordingly, the PV power increases up to its reference. In Case III, there is a relatively large deviation of the PV power from its reference after the increase of irradiance, although the error is reduced in steady-state operation. The tracking error values in all cases are relatively large, compared to other algorithms. The operating point of the PV strings under all of the cases are illustrated in the right-side of Fig. 8(a). It can be seen that *m*4 moves the operating point to the right-side of the MPP. Under the fast decrease of the irradiance, the operating point goes close to the open-circuit voltage of the PV string, which can destabilize the system.

The performance of the algorithms *m*6, *m*9 and *m*11 with

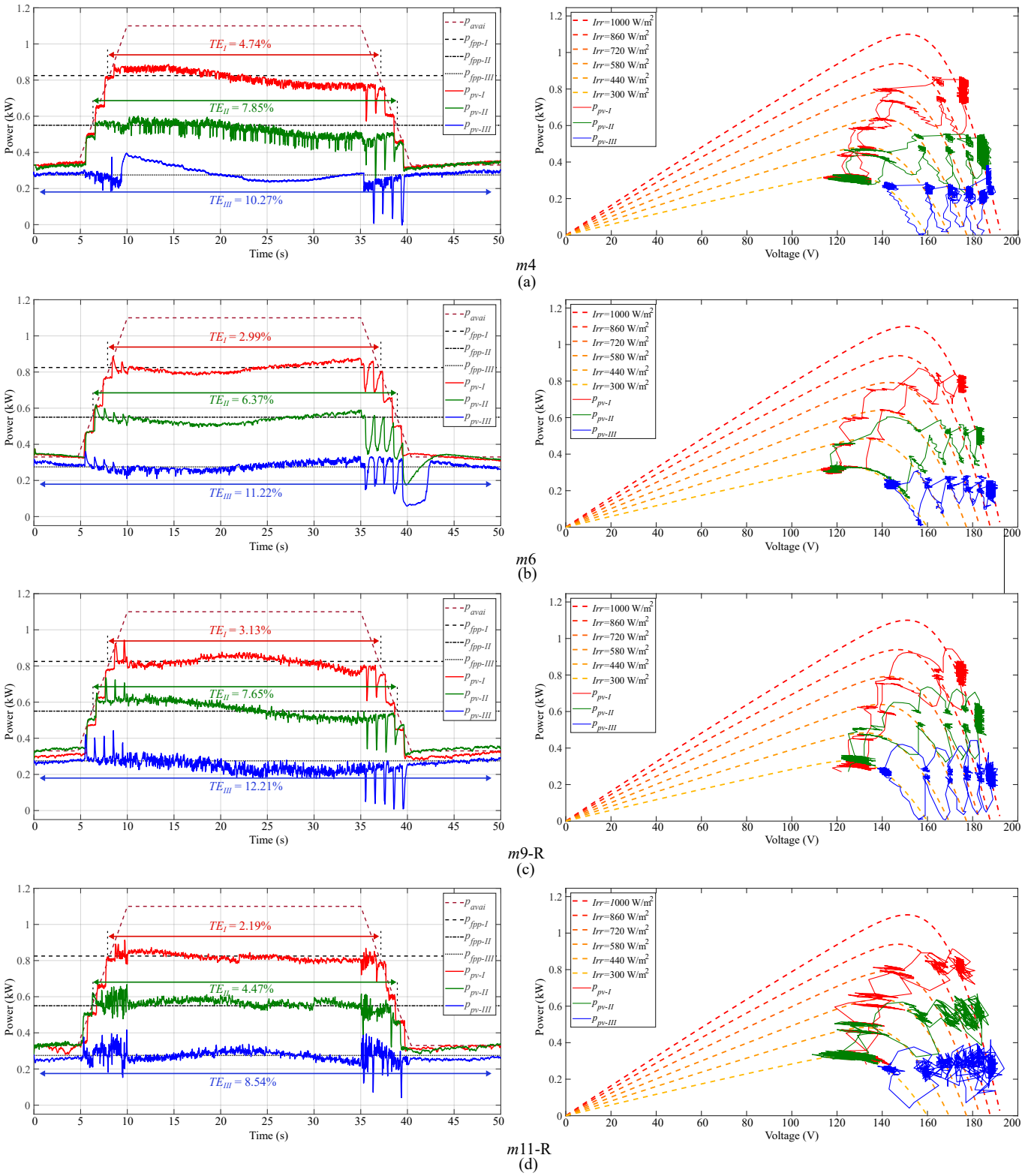

Fig. 8. Performance comparison of various FPPT under fast changes of irradiance - PV power and its references (left-side) and PV operating point (right-side) for algorithms (*Irr* - irradiance): (a) *m*4, (b) m6, (c) *m*9 with operation at the right-side of the MPP, and (d) *m*11 with operation at the right-side of the MPP.

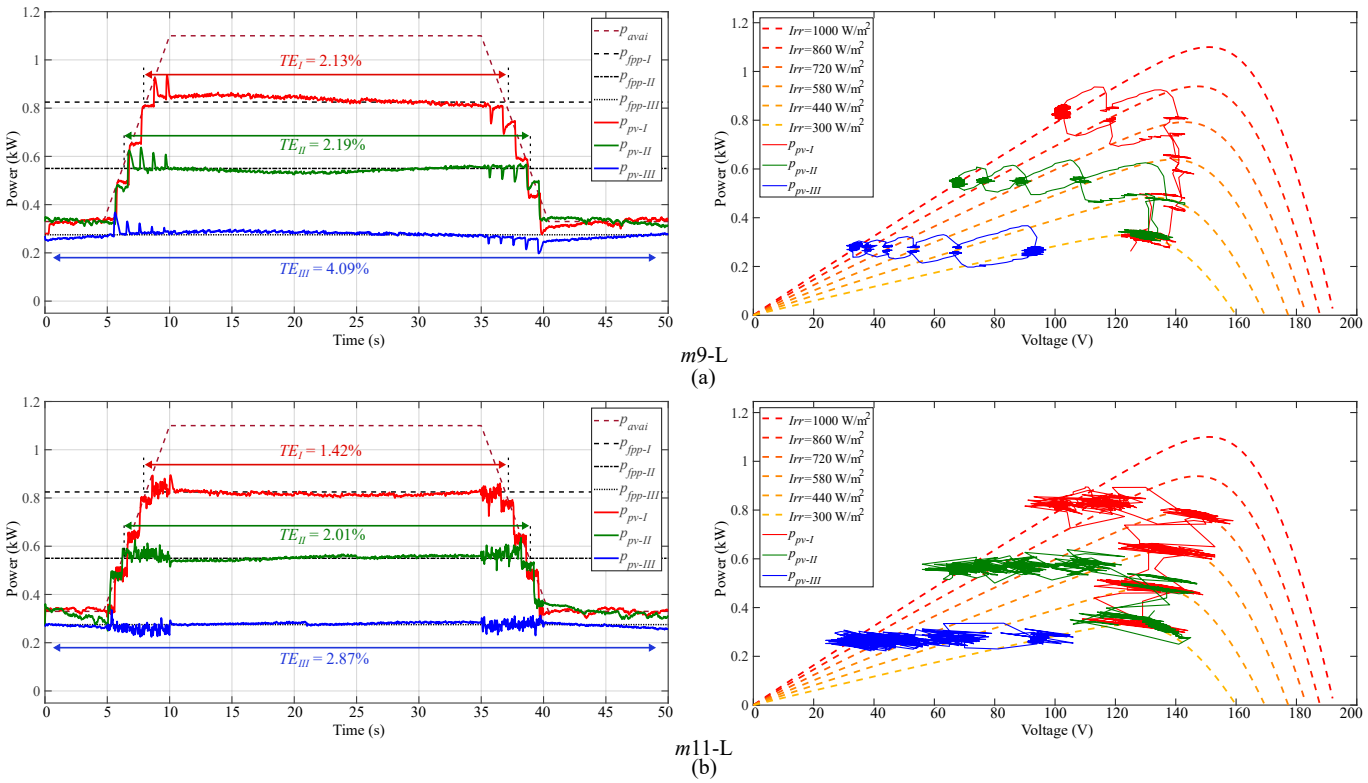

Fig. 9. Performance comparison of various FPPT under fast changes of the irradiance - PV power and its references (left-side) and PV operating point (right-side) for algorithms (*Irr* - irradiance): (a) $m9$ with operation at the left-side of the MPP, and (b) $m11$ with operation at the left-side of the MPP.

TABLE III
DESIGNED PARAMETERS OF THE INVESTIGATED ALGORITHMS.

Algorithm	Parameters
$m1$	$k_P = 0.11$, $k_I = 11.5$
$m2$	$k_P = 0.4$, $k_I = 4.5$
$m3$	$k_P = 0.5$, $k_I = 25$
$m4$	$k_{mpp} = 0.05$, $k_{FPPT} = 0.008$
$m5$	$k_P = 0.16$, $k_I = 3.3$
$m6$	$k_P = 0.16$, $k_I = 3.3$
$m7$	$k_P = 0.018$, $k_I = 50$
$m8$	$k_P = 0.018$, $k_I = 50$
$m9$-R	$V_{step\text{-}fpp} = 1.5$, $T_{step\text{-}fpp} = 0.001$
$m9$-L	$V_{step\text{-}fpp} = 6.9$, $T_{step\text{-}fpp} = 0.001$
$m10$-R	$V_{step\text{-}fpp\text{-}st} = 1.5$, $V_{step\text{-}fpp\text{-}tr} = 5.2$, $T_{step\text{-}fpp} = 0.001$
$m10$-L	$V_{step\text{-}fpp\text{-}st} = 1.5$, $V_{step\text{-}fpp\text{-}tr} = 25$, $T_{step\text{-}fpp} = 0.001$
$m11$-R	$V_{step} = 1.5$, $T_{step} = 0.001$, $k_1 = 0.006$, $k_2 = 0.05$
$m11$-L	$V_{step} = 3.1$, $T_{step} = 0.001$, $k_1 = 0.001$, $k_2 = 0.085$

the operation in the right-side of the MPP are also provided in Fig. 8. Each algorithm results in different tracking errors, which can be considered as a comparison parameter between the algorithms. The tracking error is larger for smaller power reference values, due to the large power oscillations at the right-side of the MPP. In order to tackle this problem, the algorithms $m9$ and $m11$ are proposed in the literature (see Fig. 6), which are able to directly calculate the PV voltage reference, at the left-side of the MPP. The performance of these algorithms under fast change of the irradiance is illustrated in Fig. 9. It is seen that the tracking error for the algorithm $m11$ with the operation at the left-side of the MPP is smaller than all other algorithms, for all the three case studies. One of the reasons for such a performance is the existence of relatively low power oscillations by operating at the left-side of the MPP. Another reason is the adaptive calculation of the voltage step based on the operating point and operation mode (i.e., transient or steady-state). This fact is visible by comparing the results in Fig. 9, in which Fig. 9(a) uses a constant voltage step in $m9$, and an adaptive voltage step is utilized in Fig. 9(b). Based on the performance under fast irradiance changes with different power reference values, it is seen that $m11$, which operates at the left-side of the MPP, shows a better performance compared to the other algorithms. Different features of these algorithms are analyzed and discussed in the following section.

VI. COMPARISON OF VARIOUS FPPT ALGORITHMS

This section provides a comprehensive comparison of the above mentioned FPPT algorithms. Several aspects of these algorithms including: i) ability to track the maximum power point, ii) multi-mode transition, iii) operating region in the P-V curve, iv) dynamic response, v) power oscillations in steady state, vi) performance under environmental changes, and vii)

TABLE IV
COMPARISON OF TRACKING ERROR INDICES OF THE ALGORITHMS.

Algorithm	TE_{ss} (%)	TE_{tr1} (%)	TE_{tr2} (%)	TE (%)
*m*1	5.8	3.2	63	6.6
*m*2	4.4	4.5	52	6.4
*m*3	0.5	3.1	15.4	3.2
*m*4	6.8	4.5	20.3	8.2
*m*5	4.9	3.4	18.7	6.1
*m*6	4.8	3.5	17.5	5.9
*m*7	0.6	0.6	66.8	0.9
*m*8	0.5	0.6	72.5	0.8
*m*9-R	5.2	7.1	11.3	8.8
*m*9-L	6.0	8.9	14.6	10.7
*m*10-R	5.1	2.6	10.8	5.7
*m*10-L	1.1	4.2	10.5	4.4
*m*11-R	4.0	1.7	10.7	4.4
*m*11-L	**2.1**	**2.9**	**9.2**	**3.6**

tracking error as well as the main demerits of each algorithm are analyzed in Table V.

Four indices are also defined to compare the algorithms, as follows:

- Steady-state tracking error (TE_{ss}): This index is calculated for the steady-state operation of the algorithms, in which $p_{fpp} = 500$ W and irradiance is $Irr = 1000\,^{W}/_{\mathrm{m}^2}$.
- Transient tracking error (TE_{tr1}) under step change of the power reference: This index is calculated for the transient operation of the algorithms, in which the power reference increases as a step from $p_{fpp} = 500$ W to $p_{fpp} = 1000$ W and irradiance is kept constant at $Irr = 1000\,^{W}/_{\mathrm{m}^2}$. The period of the calculation of this index is set equal to the longest period in which all the algorithms reach their new steady-state value.
- Cumulative tracking error (TE) is calculated based on (2) with including TE_{ss} and TE_{tr1}.
- Transient tracking error (TE_{tr2}) under ramp change of the irradiance. Since some of the algorithms are not able to track the power reference under environmental changes, this index is defined to differentiate the performance of the algorithms under environmental changes. The power reference is considered as $p_{fpp} = 750$ W, while the irradiance reduces linearly from $Irr = 1000\,^{W}/_{\mathrm{m}^2}$to $Irr = 400\,^{W}/_{\mathrm{m}^2}$in a period of 0.1 s.

All the algorithms are implemented and the above mentioned parameters are calculated and tabulated in Table IV.

Algorithms *m*1 and *m*2 are not able to extract the maximum available power if the available power is smaller than the power reference p_{fpp}. Hence, these algorithms are not suitable for the FPPT operation during a long period with environmental changes. Algorithms *m*3 and *m*4 require multi-mode transitions and large power oscillations occur during these mode transitions. Algorithms *m*5 and *m*6 can only implement some specific MPPT methods with current reference calculation. In these algorithms, an accurate design of the MPPT algorithm is required because the current reference calculated by this algorithm is modified in the controller, which can confuse it to move the operating point to the wrong direction. Algorithms *m*7 and *m*8 cannot be implemented for the FPPT operation for a long period. These algorithms freeze the operation of the MPPT algorithms and use the last recorded MPP voltage. Hence, it is assumed that the environmental conditions (irradiance and temperature) are not changed, which makes them applicable for a short period. In summary, each of the benchmarked algorithms with the modification of the voltage controller, as shown in Fig. 5, have several demerits for the FPPT operation. Accordingly, the algorithms with the direct calculation of the voltage reference, shown in Fig. 6, are proposed in the literature.

The main advantage of the FPPT algorithms with direct calculation of the voltage reference corresponding to p_{fpp} is that the voltage and current controller of the dc-dc converter remains the same as any conventional control algorithm and re-design and tuning of the controller is not required. The only difference between the MPPT and FPPT operation is that instead of calculating v_{mpp}, as shown in Fig. 1, v_{fpp} is calculated and fed into the voltage controller of the converter. Accordingly, the implementation of these algorithms leads to less complexity compared to the algorithms in Fig. 5. The algorithm *m*9 uses a constant voltage-step during the FPPT operation. In this case, the selection of a relatively large voltage-step results in high power oscillations during the steady state, however a small voltage-step on the other hand results in slow dynamics. This problem is solved in *m*10, which imposes two different voltage-step values during transient and steady state operation modes. The main demerit of *m*10 is that it can have large power oscillations during the steady state, according to the operation point of the PV string. In order to enhance the performance, the algorithm *m*11 implements the adaptive voltage-step calculation structure, based on the operating point and operation mode of the PV string. This algorithm achieves fast dynamics in combination with low power oscillations during the steady state operation.

Another advantage of the algorithms with the direct calculation of the voltage reference is the ability to move the operating point to both right- and left-sides of the MPP. As demonstrated in Section V, for relatively small power reference values, the operation in the right-side of the MPP results in larger power oscillations and the operation can become unstable under fast reduction of the irradiance (i.e., the operating point goes beyond the open circuit voltage of the PV string). On the other hand, moving the operating point to the left-side of the MPP achieves low power oscillations, while fast dynamics can also be obtained by using an adaptive voltage step, as implemented in the algorithm *m*11. The tracking error values, illustrated in Section V, prove the superior performance of the algorithm *m*11 compared to other available algorithms in the literature. Hence, among all the investigated algorithms, *m*11 obtains a better performance across most of the aspects. Its main demerit lies in relatively high complexity of calculations, although it

TABLE V
COMPARISON OF VARIOUS FPPT ALGORITHMS

Algorithm	Ability to track maximum power point	Multi-mode transition	Operating region	Dynamic response	Power oscillations in steady state	Ability to operate under environmental changes	Tracking Error	Computational Complexity	Main merits and demerits
*m*1 - Direct power control [51], [52]	No	No	Right	Fast	High	No	Very High	Very Low	+ Simple implementation - Not able to extract the maximum power if: $p_{avai} < p_{fpp}$. - Not applicable under environmental changes
*m*2 - PV current control with dc-link voltage stabilizer [53]	No	No	Right	Fast	High	No	Very High	Very Low	+ Simple implementation - Not able to extract the maximum power if: $p_{avai} < p_{fpp}$. - Not applicable under environmental changes
*m*3 - PV power control with inductor current reference calculation [54]	Yes	Yes	Right	Fast	High	Yes	Very High	Low	+ Low computational complexity - Large steady state power oscillations due to multi mode transitions
*m*4 - Multi-mode operation with PV voltage control [55]–[57]	Yes	Yes	Right	Fast	High	Yes	Very High	Low	- Large steady state power oscillations due to multi mode transitions
*m*5 - PV power limit control [58], [59]	Yes	No	Right	Slow	Low	Yes	High	Low	- Not applicable with various MPPT algorithms - High probability of becoming unstable under small power reference values
*m*6 - PV current limit control [58], [59]	Yes	No	Right	Slow	Low	Yes	High	Low	- Not applicable with various MPPT algorithms - High probability of becoming unstable under small power reference values
*m*7 - PV power control with dc-link voltage-based delta-voltage control [49], [60], [61]	No	Yes	Right	Slow	Low	No	High	Low	+ Applicable for two-stage PVPP and operation during voltage sag - Not applicable for long period of FPPT operation - Not applicable under environmental changes
*m*8 - PV power control with PV power-based delta-voltage control [62]	No	Yes	Right	Slow	Low	No	High	Low	- Not applicable for long period of FPPT operation - Not applicable under environmental changes
*m*9 - FPPT with constant voltage-step [32], [34], [56], [66]–[68]	Yes	Yes	Both	Slow	High	Yes	Low	High	- Slow dynamic response - High probability of becoming unstable under small power reference values
*m*10 - FPPT algorithm with different transient and steady state voltage-step values [24]	Yes	Yes	Both	Fast	Low	Yes	Low	High	- Need of multi-mode transitions
*m*11 - General FPPT algorithm with adaptive voltage-step [69]	Yes	No	Both	Fast	Low	Yes	Very Low	Very High	- Need of high computational capacity

can easily be implemented on readily-available digital signal processors.

VII. Conclusion and Future Directions

An overview of several FPPT algorithms in the literature has been presented in this paper. A short description of the algorithms has been provided, while their features have been comprehensively compared. Experimental results have also been illustrated to analyze the dynamic performance of these algorithms. The comparison reveals that the FPPT algorithms with direct calculation of the voltage reference, corresponding to the power reference, provide better performance in most of the aspects. These algorithms do not necessitate multi-mode transitions, while they are flexible to move the operation point of the PV string to the right- or left-side of the MPP. Fast dynamic response and low power oscillations in the steady state can also be achieved by adaptively calculating the voltage-step in these algorithms. Furthermore, they do not compel any change in the voltage control block of the PVPPs.

The following aspects can be regarded as future directions of this study:

- Investigating novel FPPT algorithms with the capability to operate under partial shading conditions, which is a practical problem in PVPPs.
- Estimation of the maximum available power during the FPPT operation to adjust the power reserve, without distorting the extracted power from the PV strings.
- Implementing virtual inertia and frequency response methods by considering the FPPT operation and reduced energy storage size.
- Investigating the performance of FPPT algorithms on microinverters.

References

[1] M. Morjaria, D. Anichkov, V. Chadliev, and S. Soni, "A grid-friendly plant: The role of utility-scale photovoltaic plants in grid stability and reliability," *IEEE Power and Energy Mag.*, vol. 12, no. 3, pp. 87–95, May 2014.

[2] Y. Yang, P. Enjeti, F. Blaabjerg, and H. Wang, "Wide-scale adoption of photovoltaic energy: Grid code modifications are explored in the distribution grid," *IEEE Ind. Appl. Mag.*, vol. 21, no. 5, pp. 21–31, Sep. 2015.

[3] REN21, "Renewables 2018: Global status report (GRS)," 2018. [Online]. Available: http://www.ren21.net/.

[4] X. Li, H. Wen, Y. Hu, L. Jiang, and W. Xiao, "Modified beta algorithm for GMPPT and partial shading detection in photovoltaic systems," *IEEE Trans. Power Electron.*, vol. 33, no. 3, pp. 2172–2186, Mar. 2018.

[5] G. Farivar, B. Asaei, and S. Mehrnami, "An analytical solution for tracking photovoltaic module MPP," *IEEE J. Photovoltaics*, vol. 3, no. 3, pp. 1053–1061, Jul. 2013.

[6] M. A. Danandeh and S. M. Mousavi G., "Comparative and comprehensive review of maximum power point tracking methods for PV cells," *Renew. Sustain. Energy Rev.*, vol. 82, pp. 2743–2767, Feb. 2018.

[7] L. L. Jiang, R. Srivatsan, and D. L. Maskell, "Computational intelligence techniques for maximum power point tracking in PV systems: A review," *Renew. Sustain. Energy Rev.*, vol. 85, pp. 14–45, Apr. 2018.

[8] J. P. Ram, N. Rajasekar, and M. Miyatake, "Design and overview of maximum power point tracking techniques in wind and solar photovoltaic systems: A review," *Renew. Sustain. Energy Rev.*, vol. 73, pp. 1138–1159, Feb. 2017.

[9] J. D. Bastidas-Rodriguez, E. Franco, G. Petrone, C. A. Ramos-Paja, and G. Spagnuolo, "Maximum power point tracking architectures for photovoltaic systems in mismatching conditions: a review," *IET Power Electron.*, vol. 7, no. 6, pp. 1396–1413, Jun. 2014.

[10] C. Manickam, G. P. Raman, G. R. Raman, S. I. Ganesan, and N. Chilakapati, "Fireworks enriched P&O algorithm for GMPPT and detection of partial shading in PV systems," *IEEE Trans. Power Electron.*, vol. 32, no. 6, pp. 4432 – 4443, Jun. 2017.

[11] B. Subudhi and R. Pradhan, "A comparative study on maximum power point tracking techniques for photovoltaic power systems," *IEEE Trans. Sustain. Energy*, vol. 4, no. 1, pp. 89–98, Jan. 2013.

[12] M. A. Elgendy, B. Zahawi, and D. J. Atkinson, "Assessment of perturb and observe MPPT algorithm implementation techniques for PV pumping applications," *IEEE Trans. Sustain. Energy*, vol. 3, no. 1, pp. 21–33, Jan. 2012.

[13] K. S. Tey and S. Mekhilef, "Modified incremental conductance algorithm for photovoltaic system under partial shading conditions and load variation," *IEEE Trans. Ind. Electron.*, vol. 61, no. 10, pp. 5384–5392, Oct. 2014.

[14] A. Reinhardt, D. Egarter, G. Konstantinou, and D. Christin, "Worried about privacy? let your PV converter cover your electricity consumption fingerprints," in *Proc. IEEE Inter. Conf. on Smart Grid Communications (SmartGridComm)*, pp. 25–30, Nov. 2015.

[15] Y. Yang, K. A. Kim, F. Blaabjerg, and A. Sangwongwanich, *Advances in Grid-Connected Photovoltaic Power Conversion Systems*. Woodhead Publishing, 213 pages, 2018.

[16] Y. Yang, F. Blaabjerg, H. Wang, and M. G. Simoes, "Power control flexibilities for grid-connected multi-functional photovoltaic inverters," *IET Renew. Power Gener.*, vol. 10, no. 4, pp. 504–513, Apr. 2016.

[17] "IEEE standard for interconnection and interoperability of distributed energy resources with associated electric power systems interfaces," *IEEE Std 1547-2018 (Revision of IEEE Std 1547-2003)*, Apr. 2018.

[18] G. Vahan and S. Booth, "Review of PREPA technical requirements for interconnecting wind and solar generation," *Natl. Renew. Energy Lab. (NREL), Tech. Rep. NREL/TP-5D00-57089.*, 2013.

[19] "Technical regulation 3.2.2 for PV power plants with a power output above 11 kW," *Danish grid codes*, 2015.

[20] "Transmission code 2007. network and system rules of the german transmission system operators," *V. D. N. V. E.ON Netz GmbH*, 2007.

[21] A. Cabrera-Tobar, E. Bullich-Massague, M. Aragues-Penalba, and O. Gomis-Bellmunt, "Review of advanced grid requirements for the integration of large scale photovoltaic power plants in the transmission system," *Renew. Sustain. Energy Rev.*, vol. 62, pp. 971–987, Sep. 2016.

[22] P. Hacke, S. Lokanath, P. Williams, A. Vasan, P. Sochor, G. S. Tamizh-Mani, H. Shinohara, and S. Kurtz, "A status review of photovoltaic power conversion equipment reliability, safety, and quality assurance protocols," *Renew. Sustain. Energy Rev.*, vol. 82, no. 1, pp. 1097–1112, Feb. 2018.

[23] N. A. E. R. Corporation, "BAL-003-1 frequency response and frequency bias setting standard," 2016.

[24] H. D. Tafti, A. I. Maswood, G. Konstantinou, J. Pou, and F. Blaabjerg, "A general constant power generation algorithm for photovoltaic systems," *IEEE Trans. Power Electron.*, vol. 33, no. 5, pp. 4088–4101, May 2018.

[25] A. Sangwongwanich, Y. Yang, and F. Blaabjerg, "High-performance constant power generation in grid-connected PV systems," *IEEE Trans. Power Electron.*, vol. 31, no. 3, pp. 1822–1825, Mar. 2016.

[26] R. Tonkoski, S. Member, L. A. C. Lopes, S. Member, and T. H. M. El-fouly, "Coordinated active power curtailment of grid connected PV inverters for overvoltage prevention," *IEEE Trans. Sustain. Energy*, vol. 2, no. 2, pp. 139–147, Apr. 2011.

[27] V. Gevorgian, "Highly accurate method for real-time active power reserve estimation for utility-scale photovoltaic power plants," *National Renewable Energy Laboratory (NREL/TP-5D00-73207)*, Feb. 2019.

[28] A. Sangwongwanich, Y. Yang, and F. Blaabjerg, "A sensorless power reserve control strategy for two-stage grid-connected PV systems," *IEEE Trans. Power Electron.*, vol. 32, no. 11, pp. 8559–8569, Nov. 2017.

[29] E. I. Batzelis, G. E. Kampitsis, and S. A. Papathanassiou, "Power reserves control for PV systems with real-time MPP estimation via curve fitting," *IEEE Trans. Sustain. Energy*, vol. 8, no. 3, pp. 1269–1280, Jul. 2017.

[30] A. Hoke and D. Maksimovic, "Active power control of photovoltaic power systems," in *Proc. of 1st IEEE Conf. on Technologies for Sustainability (SusTech)*, pp. 70–77, Aug. 2013.

[31] B. Craciun, T. Kerekes, D. Sera, and R. Teodorescu, "Frequency support functions in large PV power plants with active power reserves," *IEEE Trans. Emerg. Sel. Topics Power Electron*, vol. 2, no. 4, pp. 849–858, Dec. 2014.

[32] H. D. Tafti, A. I. Maswood, J. Pou, G. Konstantinou, and V. G. Agelidis, "An algorithm for reduction of extracted power from photovoltaic strings in grid-tied photovoltaic power plants during voltage sags," in *Proc. of IECON*, pp. 3018–3023, Oct. 2016.

[33] A. Q. Al-Shetwi, M. Z. Sujod, F. Blaabjerg, and Y. Yang, "Fault ride-through control of grid-connected photovoltaic power plants: A review," *Solar Energy*, vol. 180, pp. 340 – 350, Mar. 2019.

[34] A. Sangwongwanich, Y. Yang, F. Blaabjerg, and D. Sera, "Delta power control strategy for multistring grid-connected PV inverters," *IEEE Trans. Ind. Appl.*, vol. 53, no. 4, pp. 3862–3870, Jul. 2017.

[35] M. Chamana, B. H. Chowdhury, and F. Jahanbakhsh, "Distributed control of voltage regulating devices in the presence of high PV penetration to mitigate ramp-rate issues," *IEEE Trans. Smart Grid*, vol. 9, no. 2, pp. 1086–1095, Mar. 2018.

[36] B. Craciun, T. Kerekes, D. Sera, R. Teodorescu, and U. D. Annakkage, "Power ramp limitation capabilities of large PV power plants with active power reserves," *IEEE Trans. Sustain. Energy*, vol. 8, no. 2, pp. 573–581, Apr. 2017.

[37] V. Gevorgian and B. ONeill, "Advanced grid-friendly controls demonstration project for utility-scale PV power plants," *(NREL/TP-5D00-65368)*, Jan. 2016.

[38] N. Kakimoto, S. Takayama, H. Satoh, and K. Nakamura, "Power modulation of photovoltaic generator for frequency control of power system," *IEEE Trans. Energy Convers.*, vol. 24, no. 4, pp. 943–949, Dec. 2009.

[39] N. Beniwal, I. Hussain, and B. Singh, "Control and operation of a solar PV-battery-grid-tied system in fixed and variable power mode," *IET Gener., Transm. & Distr.*, vol. 12, no. 11, pp. 2633–2641, Jun. 2018.

[40] J. C. Hernandez, P. G. Bueno, and F. Sanchez-Sutil, "Enhanced utility-scale photovoltaic units with frequency support functions and dynamic grid support for transmission systems," *IET Renew. Power Gener.*, vol. 11, no. 3, pp. 361–372, Apr. 2017.

[41] E. Waffenschmidt and R. S. Hui, "Virtual inertia with PV inverters using DC-link capacitors," in *Proc. 18th European Conf. on Power Electron. and Appl. (EPE ECCE Europe)*, pp. 1–10, Sep. 2016.

[42] S. Adhikari and F. Li, "Coordinated V-f and P-Q control of solar photovoltaic generators with MPPT and battery storage in microgrids," *IEEE Trans. Smart Grid*, vol. 5, no. 3, pp. 1270–1281, May 2014.

[43] G. Delille, B. Francois, and G. Malarange, "Dynamic frequency control support by energy storage to reduce the impact of wind and solar generation on isolated power system's inertia," *IEEE Trans. Sustain. Energy*, vol. 3, no. 4, pp. 931–939, Oct. 2012.

[44] A. Saez-de-Ibarra, A. Milo, H. Gaztanaga, V. Debusschere, and S. Bacha, "Co-optimization of storage system sizing and control strategy for intelligent photovoltaic power plants market integration," *IEEE Trans. Sustain. Energy*, vol. 7, no. 4, pp. 1749–1761, Oct. 2016.

[45] "Grid-connected PV systems: Design and installation training manual," *AS/NZS 4777.2*, 2015.

[46] BDEW, "Technical guideline - generating plants connected to the medium-voltage network," *Germany grid codes*, 2008.

[47] N. E. R. of South Africa (NERSA), "Grid connection code for renewable power plants connected to the electricity transmission system or the distribution system in south africa," *Technical Report, NERSA, South Africa*, 2012.

[48] S. Kouro, J. I. Leon, D. Vinnikov, and L. G. Franquelo, "Grid-connected photovoltaic systems: An overview of recent research and emerging PV converter technology," *IEEE Ind. Electron. Mag.*, vol. 9, no. 1, pp. 47–61, Mar. 2015.

[49] M. Mirhosseini, J. Pou, and V. G. Agelidis, "Single- and two-stage inverter-based grid-connected photovoltaic power plants with ride-through capability under grid faults," *IEEE Trans. Sustain. Energy*, vol. 6, no. 3, pp. 1150–1159, Jul. 2015.

[50] M. Mirhosseini, J. Pou, B. Karanayil, and V. G. Agelidis, "Resonant versus conventional controllers in grid-connected photovoltaic power plants under unbalanced grid voltages," *IEEE Trans. Sustain. Enery*, vol. 7, no. 3, pp. 1124–1132, Jul. 2016.

[51] C. Rosa, D. Vinikov, E. Romero-Cadaval, V. Pires, and J. Martins, "Low-power home PV systems with MPPT and PC control modes," in *Proc. of Intern. Conf.-Workshop Compatibility in Power Electron. (CPE)*, pp. 58–62, Jun. 2013.

[52] S. M. Park and S. Y. Park, "Power weakening control of the photovoltaic-battery system for seamless energy transfer in microgrids," in *Proc. of APEC*, pp. 2971–2976, Mar. 2013.

[53] C. Y. Tang, Y. T. Chen, and Y. M. Chen, "PV power system with multi-mode operation and low-voltage ride-through capability," *IEEE Trans. Ind. Electron.*, vol. 62, no. 12, pp. 7524–7533, Dec. 2015.

[54] A. Urtasun, P. Sanchis, and L. Marroyo, "Limiting the power generated by a photovoltaic system," in *Proc. 10th Intern. Multi-Conf. on Systems, Signals and Devices (SSD)*, pp. 1–6, 2013.

[55] Y. Yang, F. Blaabjerg, and H. Wang, "Constant power generation of photovoltaic systems considering the distributed grid capacity," in *Proc. of APEC*, pp. 379–385, Mar. 2014.

[56] Y. Yang, H. Wang, F. Blaabjerg, and T. Kerekes, "A hybrid power control concept for PV inverters with reduced thermal loading," *IEEE Trans. Power Electron.*, vol. 29, no. 12, pp. 6271–6275, Dec. 2014.

[57] H. D. Tafti, C. D. Townsend, G. Konstantinou, and J. Pou, "A multi-mode flexible power point tracking algorithm for photovoltaic power plants," *IEEE Trans. Power Electron.*, vol. 34, no. 6, pp. 5038–5042, Jun., 2019.

[58] A. Sangwongwanich, Y. Yang, F. Blaabjerg, and H. Wang, "Benchmarking of constant power generation strategies for single-phase grid-connected photovoltaic systems," *IEEE Trans. Ind. Appl.*, vol. 54, no. 1, pp. 447–457, Jan. 2018.

[59] A. Sangwongwanich, Y. Yang, F. Blaabjerg, and H. Wang, "Benchmarking of constant power generation strategies for single-phase grid-connected photovoltaic systems," in *Proc. of APEC*, pp. 370–377, Mar. 2016.

[60] H. D. Tafti, A. Maswood, G. Konstantinou, J. Pou, K. Kandasamy, Z. Lim, and G. H. P. Ooi, "Study on the low-voltage ride-thorough capability of photovoltaic grid-connected neutral-point-clamped inverters with active/reactive power injection," *IET Renew. Power Gener.*, vol. 11, no. 8, pp. 1182–1190, Jul. 2017.

[61] H. D. Tafti, A. I. Maswood, Z. Lim, G. H. P. Ooi, and P. H. Raj, "NPC photovoltaic grid-connected inverter with ride-through capability under grid faults," in *Proc. IEEE 11th Intern. Conf. on Power Electron. and Drive Sys.*, pp. 518–523, Jun. 2015.

[62] H. Tafti, A. Maswood, G. Konstantinou, J. Pou, and P. Acuna, "Active/reactive power control of photovoltaic grid-tied inverters with peak current limitation and zero active power oscillation during unbalanced voltage sags," *IET Power Electron.*, vol. 11, no. 6, May 2018.

[63] C. Rosa, D. Vinikov, E. Romero-Cadaval, V. Pires, and J. Martins, "Low-power home PV systems with MPPT and PC control modes," in *Proc. Int. Conf.-Workshop Compatibility And Power Electron.*, pp. 58–62, Jun. 2013.

[64] A. Hoke and D. Maksimovic, "Active power control of photovoltaic power systems," in *Proc. IEEE 1st Conf. on Technologies for Sustainability (SusTech)*, pp. 70–77, Aug. 2013.

[65] R. G. Wandhare and V. Agarwal, "Precise active and reactive power control of the PV-DGS integrated with weak grid to increase PV penetration," in *Proc. IEEE 40th Photovoltaic Specialist Conf. (PVSC)*, pp. 3150–3155, Jun. 2014.

[66] A. Ahmed, L. Ran, S. Moon, and J. H. Park, "A fast PV power tracking control algorithm with reduced power mode," *IEEE Trans. Energy Convers.*, vol. 28, pp. 565–575, Sep. 2013.

[67] Y. Yang, E. Koutroulis, A. Sangwongwanich, and F. Blaabjerg, "Pursuing photovoltaic cost-effectiveness: Absolute active power control offers hope in single-phase PV systems," *IEEE Ind. Appl. Mag.*, vol. 23, no. 5, pp. 40–49, Jun. 2017.

[68] Y. Yang and F. Blaabjerg, "Overview of single-phase grid-connected photovoltaic systems," *Electr. Power Compon. and Syst.*, vol. 43, no. 12, pp. 1352–1363, Jul. 2015.

[69] H. D. Tafti, A. Sangwongwanich, Y. Yang, G. Konstantinou, J. Pou, and F. Blaabjerg, "A general algorithm for flexible active power control of

photovoltaic systems," in *Proc. of APEC*, pp. 1115–1121, Mar. 2018.

Hossein Dehghani Tafti (S'13–M'18) received the B.Sc. and M.Sc. degrees in electrical engineering and power system engineering from the Amirkabir University of Technology, Tehran, Iran, in 2009 and 2011, respectively, and the Ph.D. degree in electrical engineering from the Nanyang Technological University, Singapore, in 2018. From February 2016 to August 2016, he was on a research exchange program with the University of New South Wales, Sydney, NSW, Australia, where he was working on the control of multilevel grid-connected converters. From August 2017 to October 2017, he was a Researcher with Aalborg University, Aalborg, Denmark, where he was working on the flexible power point tracking in photovoltaic power plants. Since March 2018, he is a research fellow at Nanyang Technological University. He was co-editor of the book titled "Advanced multilevel converters and applications in grid integration", published by John Wiley in 2018. His research interest includes the grid-integration of renewable energy sources, in particular, photovoltaics and energy storage and design and control of multilevel power converters.

Georgios Konstantinou (S'08–M'11–SM'18) received the B.Eng. degree in electrical and computer engineering from the Aristotle University of Thessaloniki, Thessaloniki, Greece, in 2007 and the Ph.D. degree in electrical engineering from UNSW Sydney (The University of New South Wales), Australia, in 2012. From 2012 to 2015 he was a Research Associate at UNSW. He is currently a Senior Lecturer with the School of Electrical Engineering and Telecommunications at UNSW Sydney and an Australian Research Council (ARC) Early Career Research Fellow. His main research interests include multilevel converters, power electronics in HVDC, renewable energy and energy storage applications. He is an Associate Editor for IEEE Transactions on Power Electronics and IET Power Electronics.

Christopher D. Townsend (S'09-M'13) received the B.E. (2009) and Ph.D. (2013) degrees in electrical engineering from the University of Newcastle, Australia. Subsequently he spent three years working at ABB Corporate Research, Sweden working on next-generation high-power converter technologies. Since then he has held various post-doctoral research positions including at the University of New South Wales, Australia, the University of Newcastle, Australia and Nanyang Technological University, Singapore. In 2019, he joined the Department of Electrical, Electronic and Computer Engineering at the University of Western Australia as a Senior Lecturer. He has authored more than 60 published technical papers and has been involved in several industrial projects and educational programs in the field of power electronics. His research interests include topologies and modulation strategies for multilevel converters applied in power systems, renewable energy integration and electric vehicle applications. Dr. Townsend is a member of the IEEE Power Electronics and Industrial Electronics societies.

Glen G. Farivar (S'13-M'17) received the B.Sc. degree in electrical engineering from Nooshirvani Institute of Technology, Babol, Iran, in 2008, the M.Sc degree in power electronics from the University of Tehran, Tehran, Iran in 2011, and PhD in electrical engineering from the University of NSW Australia, Syndey, Australia in 2016. He is currently working as a post-doctoral research fellow at the Energy Research Institute, Nanyang Technological Institute (ERI@N), Singapore. His research interests include renewable energy systems, high power convertors, energy storage, FACTS devices, and hybrid electric vehicles.

Ariya Sangwongwanich (S'15-M'19) received the M.Sc. and Ph.D. degree in energy engineering from Aalborg University, Denmark, in 2015 and 2018, respectively. Currently, he is working as a Postdoc Fellow at the Department of Energy Technology, Aalborg University. He was a Visiting Researcher with RWTH Aachen, Aachen, Germany from September to December 2017. His research interests include control of grid-connected converter, photovoltaic systems, reliability in power electronics and multilevel converters. He has co-authored the book - Advanced in Grid-Connected Photovoltaic Power Conversion Systems. In 2019, he received the Danish Academy of Natural Sciences' Ph.D. prize and the Spar Nord Foundation Research Award for his Ph.D. thesis. Dr. Sangwongwanich also serves as the Chair of the IEEE Student Branch at Aalborg University.

Yongheng Yang (SM'17) received the B.Eng. degree in electrical engineering and automation from Northwestern Polytechnical University, Shaanxi, China, in 2009 and the Ph.D. degree in electrical engineering from Aalborg University, Aalborg, Denmark, in 2014.

He was a postgraduate student at Southeast University, China, from 2009 to 2011. In 2013, he spent three months as a Visiting Scholar at Texas A&M University, USA. Dr. Yang is currently an Associate Professor with the Department of Energy Technology, Aalborg University. His current research is on the integration of grid-friendly photovoltaic systems with an emphasis on the power electronics converter design, control, and reliability.

Dr. Yang is the Chair of the IEEE Denmark Section. He serves as an Associate Editor for several prestigious journals, including the IEEE JOURNAL OF EMERGING AND SELECTED TOPICS IN POWER ELECTRONICS, the IEEE TRANSACTIONS ON INDUSTRIAL ELECTRONICS, and the IEEE TRANSACTIONS ON POWER ELECTRONICS. He is a Subject Editor of the IET Renewable Power Generation for Solar Photovoltaic Systems, including MPPT. Dr. Yang is the General Co-chair of the IEEE International Future Energy Challenge (IFEC 2020) and a Publicity Co-chair of the IEEE Energy Conversion Congress and Exposition (ECCE 2020). He was the recipient of the 2018 IET Renewable Power Generation Premium Award and was an Outstanding Reviewer for the IEEE TRANSACTIONS ON POWER ELECTRONICS in 2018.

Josep Pou (S'97-M'03-SM'13-F'17) received the B.S., M.S., and Ph.D. degrees in electrical engineering from the Technical University of Catalonia (UPC)-Barcelona Tech, in 1989, 1996, and 2002, respectively.

In 1990, he joined the faculty of UPC as an Assistant Professor, where he became an Associate Professor in 1993. From February 2013 to August 2016, he was a Professor with the University of New South Wales (UNSW), Sydney, Australia. He is currently a Professor with the Nanyang Technological University (NTU), Singapore, where he is Program Director of Power Electronics at the Energy Research Institute at NTU (ERI@N) and co-Director of the Rolls-Royce at NTU Corporate Lab. From February 2001 to January 2002, and February 2005 to January 2006, he was a Researcher at the Center for Power Electronics Systems, Virginia Tech, Blacksburg. From January 2012 to January 2013, he was a Visiting Professor at the Australian Energy Research Institute, UNSW, Sydney. He has authored more than 320 published technical papers and has been involved in several industrial projects and educational programs in the fields of power electronics and systems. His research interests include modulation and control of power converters, multilevel converters, renewable energy, energy storage, power quality, HVDC transmission systems, and more-electrical aircraft and vessels.

He is co-Editor-in-Chief of the IEEE Transactions on Industrial Electronics and Associate Editor of the IEEE Journal of Emerging and Selected Topics in Power Electronics. He received the 2018 IEEE Bimal Bose Award for Industrial Electronics Applications in Energy Systems.

Frede Blaabjerg (S'86-M'88-SM'97-F'03) was with ABB-Scandia, Randers, Denmark, from 1987 to 1988. From 1988 to 1992, he got the PhD degree in Electrical Engineering at Aalborg University in 1995. He became an Assistant Professor in 1992, an Associate Professor in 1996, and a Full Professor of power electronics and drives in 1998. From 2017 he became a Villum Investigator. He is honoris causa at University Politehnica Timisoara (UPT), Romania and Tallinn Technical University (TTU) in Estonia.

His current research interests include power electronics and its applications such as in wind turbines, PV systems, reliability, harmonics and adjustable speed drives. He has published more than 600 journal papers in the fields of power electronics and its applications. He is the co-author of four monographs and editor of ten books in power electronics and its applications.

He has received 32 IEEE Prize Paper Awards, the IEEE PELS Distinguished Service Award in 2009, the EPE-PEMC Council Award in 2010, the IEEE William E. Newell Power Electronics Award 2014, the Villum Kann Rasmussen Research Award 2014, the Global Energy Prize in 2019 and the 2020 IEEE Edison Medal. He was the Editor-in-Chief of the IEEE TRANSACTIONS ON POWER ELECTRONICS from 2006 to 2012. He has been Distinguished Lecturer for the IEEE Power Electronics Society from 2005 to 2007 and for the IEEE Industry Applications Society from 2010 to 2011 as well as 2017 to 2018. In 2019-2020 he serves a President of IEEE Power Electronics Society. He is Vice-President of the Danish Academy of Technical Sciences too. He is nominated in 2014-2019 by Thomson Reuters to be between the most 250 cited researchers in Engineering in the world.